Desalination and Water Treatment
www.deswater.com
doi: 10.5004/dwt.2021.27011

220 (2021) 199–210
April

Removal mechanisms of Cd(II) and Pb(II) from aqueous solutions using straw biochar: batch study, Raman and X-ray photoelectron spectroscopy techniques

Qingzhou Zhao[a,b], Yanfen Wang[c], Zhihong Xu[a], Zhisheng Yu[b,*]

[a]*Environmental Futures Research Institute, Griffith University, Nathan QLD 4111, Australia, emails: zqz1992@hotmail.com (Q. Zhao), zhihong.xu@griffith.edu.au (Z. Xu)*
[b]*College of Resources and Environment, University of Chinese Academy of Sciences, 19 A Yuquan Road, Shijingshan District, Beijing 100049, China, Tel. +86 10 88256057; email: yuzs@ucas.ac.cn (Z. Yu)*
[c]*College of Life Science, University of Chinese Academy of Sciences, 19 A Yuquan Road, Beijing 100049, China, email: yfwang@ucas.ac.cn*

Received 13 July 2020; Accepted 31 December 2020

ABSTRACT

Recent interests in aqueous cadmium and lead removal has been driven by the rapid progress of the adsorption on biochar, which is an environmentally friendly adsorbent with high effectiveness. The biochar was prepared from pyrolysis of straw under 400°C and characterized by scanning electron microscopy, transmission electron microscopy, energy-dispersive X-ray spectroscopy, X-ray photoelectron spectroscopy, Brunauer–Emmett–Teller, Fourier-transform infrared spectroscopy and Raman spectra analysis. The batch experiments were performed to investigate the capacity and mechanism of the adsorption. The kinetic of either Cd(II) or Pb(II) adsorption fitted in both pseudo-first-order kinetic model and pseudo-second-order kinetic model. The adsorption capacity increased rapidly in the initial 30 min and then slowed down until the plateau after 80 min. Both the capacity of the Cd(II) and Pb(II) removal increased with pH value elevation at the relatively low pH range while the Pb(II) adsorption capacity decreased with pH value elevation in the range of 8.5–11.0. Nevertheless, these adsorptions were independent of the ionic strength. Either Cd(II) or Pb(II) adsorption process fitted the Langmuir model and Freundlich model well. The thermodynamic data demonstrated the cadmium adsorption on biochar as the endothermic and spontaneous reaction with the $\Delta H° = 21.31$, $\Delta S° = 136.77$ and $\Delta G° < 0$ at 293, 313 and 333 K. The lead adsorption exhibited similar natures with $\Delta H° = 17.20$, $\Delta S° = 127.92$ and $\Delta G° < 0$. Thus, biochar would be a green material as the potential adsorbent for the cadmium and lead removal in aqueous solutions.

Keywords: Biochar; Adsorption mechanism; Cadmium; Lead

1. Introduction

The acceleration of industrial development brings about the serious problem of heavy metal contamination. Especially, the accumulation of cadmium (Cd) and lead (Pb) in water has aroused great concern owing to the environmental and ecological risk of these heavy metals [1,2]. Cadmium is a common heavy metal contaminant threatening human health as a carcinogen via the alimentary and respiratory canal [3]. Lead is another typical heavy metal pollutant primarily causes the mental, neural and behavioral problem [4–6]. To eliminate this potential impact, efficient treatment methods have been attempted to remove the Cd(II) and Pb(II) in the water body. Most of the methods can be

* Corresponding author.

classified into the electrochemical method, physiochemical method, the current method, adsorption and so on [7]. Adsorption is most widely used among these methods due to its high selectivity, low cost and operational ease [8,9]. Numerous materials are tested extensively as the absorbent in the heavy metal adsorption process. However, Cd(II) and Pb(II) removal are still limited by the adsorption capacity and manufacture of the absorbent. Thus, it is urgent to seek a more effective and easily prepared absorbent.

Biochar, the carbonaceous residue derived from the pyrolysis of biomass, is increasingly considered as the potential prevalent absorbent for heavy metal contamination. Biochar is prepared by the thermal degradation of carbon-rich feedstock in an oxygen-limited environment. A primary mechanism of the biochar adsorption is sorbing the positive metal ion with its negative surface by electronic attraction [10]. Furthermore, numerous ligands and functional groups on the biochar surface contribute to the interaction with the heavy metal into composites and participates [11–13]. Biochar is fairly similar to the activated carbon, which is the currently most commonly used carbonaceous material sorbent, in terms of the production properties via pyrolysis such as high microporosity, surface heterogeneity and superficial area [11,14]. Nevertheless, contrasted to activated carbon, biochar is generally applied in the adsorption without any thermal or chemical activation treatment to strengthening the surface characteristic [14–16]. Additionally, the chemical, physical and mechanical properties of biochar vary with the preparing condition such as feedstock type, pyrolysis temperature and retention time [14,17]. This trait provided the opportunity to optimize the most efficacious sorbent and extend the applicability of biochar. Hence, biochar can be extensively applied as a sustainable, potent and low-cost absorbent for heavy metals. Although large amount of research about the adsorption of biochar on metal ions have been carried out in previous studies, knowledge about the comparison between the biochar treatment on aqueous Cd(II) and Pb(II) contamination is limited. Studies on the role of biochar structure and characteristics in adsorption mechanisms also lag behind [18–22]. In addition, current studies on Cd(II) and Pb(II) removal were mainly based on the simulant contaminant solution while the potential efficiency of the adsorbent in actual wastewater remains unknown.

Therefore, this work aims to clarify the capacity and mechanism of the Cd(II) and Pb(II) removal by biochar adsorption and the discrepancy between these adsorptions. To achieve these objectives, biochar prepared by wheat straw was characterized by scanning electron microscopy (SEM), energy-dispersive X-ray spectroscopy (EDS), transmission electron microscopy (TEM), X-ray photoelectron spectroscopy (XPS), Brunauer–Emmett–Teller (BET), Fourier-transform infrared spectroscopy (FTIR) and Raman spectra respectively. The effects, contact time, temperature of pH and ionic strength on the adsorption process of biochar for Cd(II) and Pb(II) were determined in a batch mode. The adsorption kinetics, thermodynamic derived from the temperature adsorption isotherms, and the adsorption mechanism were also investigated. The comparison between Cd(II) and Pb(II) removal efficiency of biochar in simulant and actual wastewater was also performed.

2. Method and material

2.1. Biochar preparation

Wheat (*Triticum aestivum*) straws were collected as the feedstock of biochar. All these straws were dried by the oven at 60°C for 24 h (Fig. 1). Biochar was produced by pyrolysis with the condition of a temperature of 400°C and retention time of 2 h in an oxygen-insulated environment. The whole preparation process took place in a custom-made stainless-steel furnace. The prepared biochar was sieved with a 0.2 mm sieve for the subsequent characterization and batch experiments.

2.2. Biochar characterization

The surface functional groups were determined by Fourier-transform infrared spectroscopy (FTIR, Thermo Nicolet, 8700, Madison, WI, USA) with the scan range of 4,000–400 cm^{-1} and Raman spectra (Mettler Toledo, Zürich, Switzerland). The morphological images were derived by scanning electron microscopy (SEM, 15 JSM-6360LV) and transmission electron microscopy (TEM, JEM-1011). The element analysis was conducted by the X-ray photoelectron spectroscopy (XPS, Thermo ESCALAB 250 analyzer) with a monochromatized Al K alpha X-ray (hm = 1,486.6 eV) as the radiation source and a constant pass energy of 20 eV. The binding energies of the photoelectrons were calibrated by the C1s peak at 284.6 eV while the peak of O1s occurred at 532.7 eV.

2.3. Batch experiment

Batch adsorption experiments were investigated using aqueous cadmium and lead solution in the polyethylene centrifuge tubes without any attempt to regulate the ambient condition or remove the air among all the experiments. These performances of biochar in Cd(II) and Pb(II) adsorption with the function of contact time, initial concentration, pH, ion strength and temperature were also determined. The biochar was suspended in a solution of $NaNO_3$ for pre-equilibrium as the background electrolyte [9,23,24]. Then the stock solutions of Cd(II) and Pb(II) were added into the biochar mixed electrolyte solution to achieve the desired initial concentration of different metal components. The target system pH adjustment was conducted by adding the negligible volume of 0.01 and 0.1 mol L^{-1}

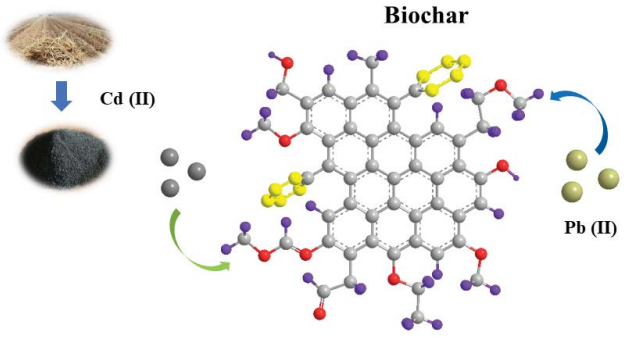

Fig. 1. Cd(II) and Pb(II) adsorption mechanism on biochar.

NaOH or HCl solution to obtain the solution with pH from 2.1 to 10.4, which is a suitable range for the metal adsorption [6,9]. To acquire the adsorption equilibrium, the polyethylene test tubes were shaken using an end-over-end tumbler. Sample tubes were shaken for 10, 20, 30, 40, 50, 60, 70, 80, 90, 100, 110 and 120 min at the temperature of 293 K, 313 K and 333 K respectively to investigate the kinetics and isotherms. The experiment for kinetics were also performed with the initial metal ion concentration of 10, 25, 50 and 70 g mL^{-1} (pH = 5.0, temperature = 293 K). Then the solid and liquid phases were separated by centrifugation at 9,000 rpm for 40 min. The concentration of the Cd(II) and Pb(II) was measured with spectrophotometry tool (spectrophotometer UV, 2600i (Shimadzu, Kyoto, Japan), λ = 228.8 nm for Cd, λ = 283.3 nm for Pb 1 cm glass cell, against distilled water). The specific surface area of the biochar was calculated according to BET adsorption/desorption curves recorded in the nitrogen atmosphere to monitor the porosity of this adsorbent. In view of the expected Cd(II) and Pb(II) loss from biochar adsorption procedure on the centrifuge tube wall, the calibration curves were obtained separately by control treatment without biochar under otherwise identical conditions. Taking the attained calibration curves into consideration, the Cd(II) and Pb(II) adsorbed mass was computed via deducting the solution mass from the mass spiked. All the experimental data are collected by the repeated measurements or the average of triplicate. The fractional errors of the data were in 5%.

3. Result and discussion

3.1. Characterization

3.1.1. Scanning electron microscopy, transmission electron microscopy and energy-dispersive X-ray spectroscopy

The SEM and TEM images before and after the Cd(II) and Pb(II) adsorption were exhibited to explicitly demonstrate the porous structure of the biochar (Fig. 2). Because of the slow pyrolysis, all the biochar before or after the sorption processes possessed the characteristics such as porous structure and opening shapes, which are important for the metal removal from aqueous solution. The intra pores provide permeable structure for the biochar to make it continuously bind the Cd(II) and Pb(II) ions even if the functional groups on the biochar surface were occupied. The raw biochar without adsorption reaction possessed quite smooth pore walls. However, after equilibrium of Cd(II) and Pb(II) in the metal removal processes, these pore walls were covered with the precipitation and came into the rough surface, which might be caused by coating of the metal ions and corrosion of the biochar [25]. The EDS spectrum for the raw biochar depicted no peak characteristics of Cd(II) or Pb(II) (Fig. S1). However, after the adsorption was processed for these two elements, new peak characteristics of Cd(II) or Pb(II) were observed respectively. These results pointed out that the sorption led by ion exchange on biochar surface explained the aqueous metal

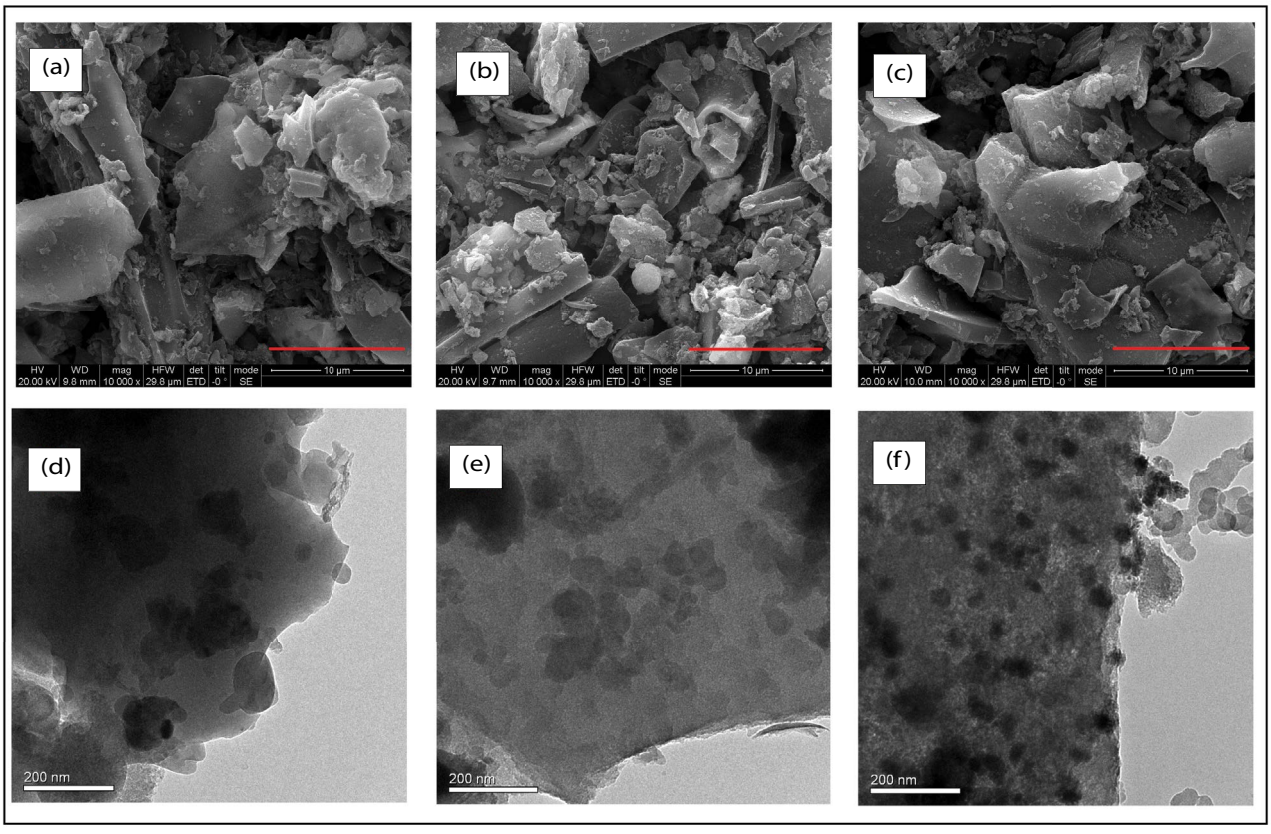

Fig. 2. Scanning electron microscope (SEM) and transmission electron microscope (TEM) images of biochar before (a and d) and after (b, c, e, f) reaction.

removal. The bindings of the two metal ions to biochar also could be confirmed by these EDS spectrum results.

3.1.2. FTIR and Raman spectrum analysis

The FTIR and Raman spectra were characterized to investigate the functional groups on the surface of biochar. The FTIR spectra in the range of 400–4,000 were observed before and after the Cd(II) or Pb(II) removal processes (Fig. 3a). Several functional groups such as O–H, C–H, C–O and C–C which participated in absorbing heavy metal ions were observed on the raw biochar. The broad peak at 3,318.57 exhibited the presence of O–H stretching vibration correlated to a hydroxyl group in ethanol or phenol; the axial deformation attributed to strong C–O vibration at 1,095.57 represented another two hydroxyl group. The peaks observed at 1,430.35 and 796.30 showed C–H bending vibration corresponded to aliphatic and aromatic hydrocarbon and alkene; the C–C vibration at 465.64 was assigned to aromatic hydrocarbon [25,26]. These functional groups distinctly revealed the complex nature of biochar surface. After adsorption processed for Cd(II) or Pb(II) removal, all the intensities of the peaks corresponding to these functional groups decreased, which indicated that surface complexity led by the O–H, C–H, C–O and C–C groups play a vital role in the adsorption reaction. Especially, peak areas of C–O and C–C groups showed the most acute reduction. It proved the presence of chemical reactions involving these groups in the adsorption process.

The Raman spectra of the biochar in the wavelength region of 500–2,000 before and after the Cd(II) or Pb(II) adsorption are exhibited in Fig. 3b. Peaks representing D and G bands were observed at 1,368–1,384 cm^{-1} and 1,588–1,600 cm^{-1}. After the adsorption process, obvious change of the G bands representing vibrations of sp2 carbon atoms clearly showed in Fig. 6 indicated the participation of the sp2 carbon, which could be imputed to π electrons interaction mechanisms. It reflected the graphitic nature and double bonds of biochar. Meanwhile, the variant D band peak and D/G ratio revealed the breathing modes of disordered graphite rings [27,28].

3.1.3. XPS analysis

Similar results were found in the determination for XPS spectra of C1s before and after the adsorption of the aqueous Cd(II) or Pb(II) in Fig. 4. Peaks representing C–C (sp^2-carbon) C–C (sp^3-carbon) were classified at the binding energy of 284.4 eV and 284.8 eV. All the peaks of C–C groups before or after Cd(II) or Pb(II) adsorption attributed the majority of the carbon functional groups (raw biochar: 76.00%, biochar+Cd:67.79%, biochar+Pb:66.88%). The peaks at 285.4 eV after the metal ion removal also showed resemble distribution with raw biochar (raw biochar: 18.06%, biochar+Cd:16.84%, biochar+Pb:19.14%) [25,29]. However, compared to the raw biochar the relative percentage of carbonyl groups C–O–C increased after the Cd(II) or Pb(II) removal (raw biochar: 5.94%, biochar+Cd:15.37%, biochar+Pb:14.01%). It might be attributed to the chemical redox reactions which formed C–O–C groups. This finding also indicated the important role of surface complexation in the Cd(II) or Pb(II) adsorption [29]. In the O1s XPS spectra for the raw biochar, the peak of carbonyl groups C=O at 531.5 eV might indicate the presence of the ketone, lactone, carbonyl, and quinine groups. Peaks representing C–O and O–C=O (carbonyl bond in the carboxylic group) at 533.5 eV and 532.6 eV were also observed [30] (Fig. 4d). A similar distribution of these oxygen functional groups was found in the XPS spectra for the adsorbent after Pb(II) adsorption (Fig. 4f). Nevertheless, Fig. 3e shows that the relative percentage of C=O and C–O groups decreased and the respectively after Cd(II) removal. Taking the peaks of Cd–CO_3 and Cd–$(OH)_2$ in this process into consideration depicted that C=O and C–O groups on biochar surface might play a great role in the chemical adsorption for the $CdCO_3$ and $Cd(OH)_2$ (Fig. S2). As for the Pb removal process, the chemical adsorption of $PbCO_3$ could be attributed to the carbonyl groups C–O–C rather than other oxygen containing functional groups (Fig. S3).

3.1.4. BET analysis

As an important porosity parameter, the specific surface area of the obtained biochar was calculated with the

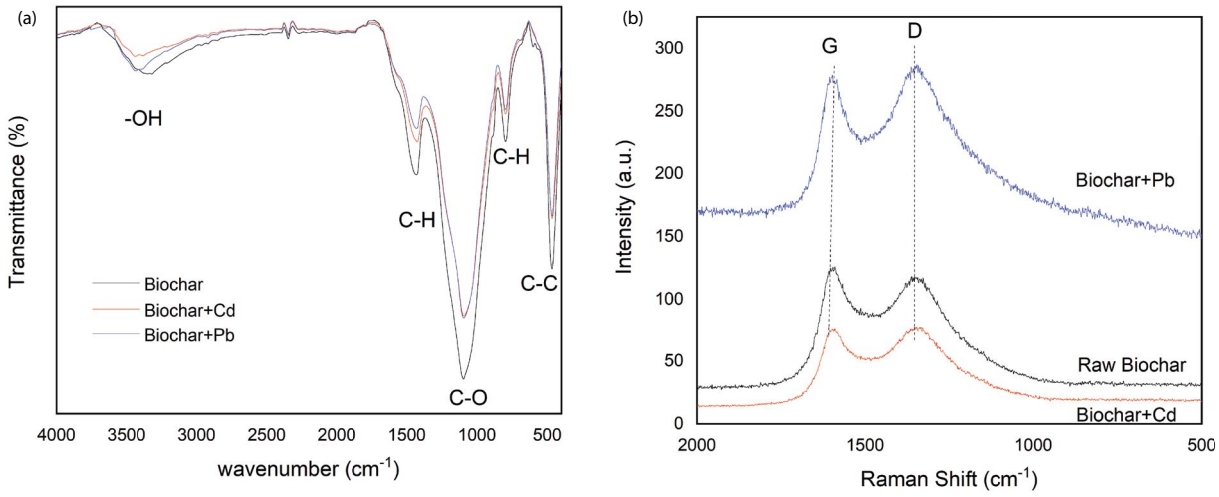

Fig. 3. FT-IR (a) and Raman (b) spectra of biochar before and after reaction.

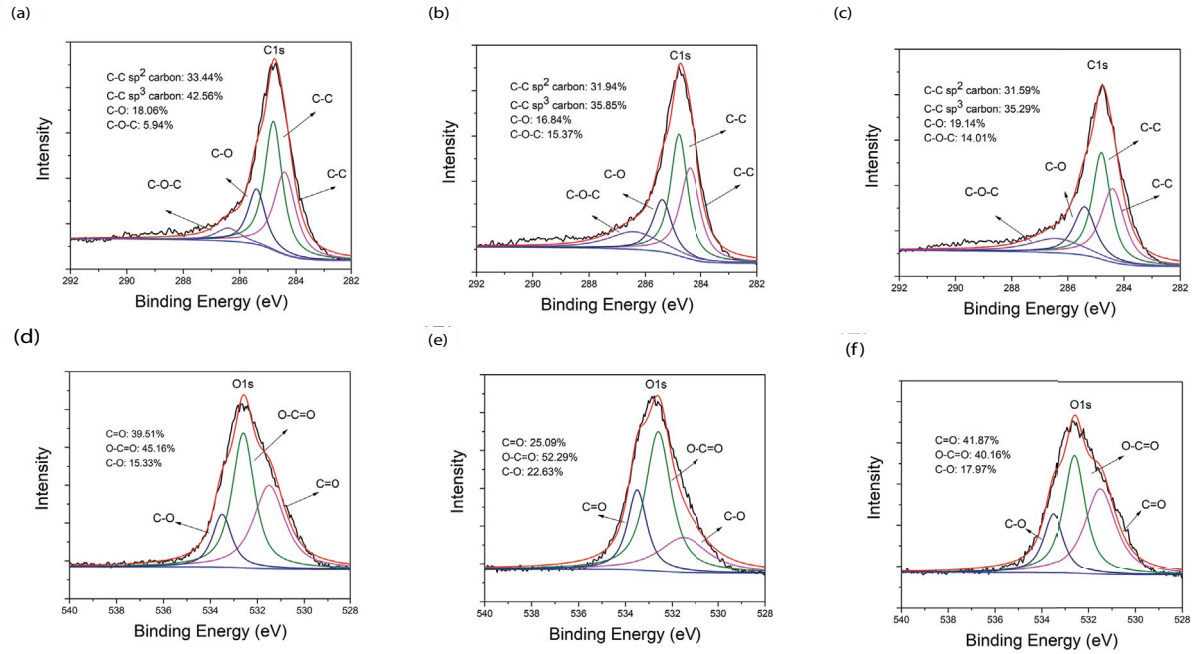

Fig. 4. High resolution X-ray photoelectron spectroscopy (XPS) spectra of C1 s before (a) and after reaction (b, c) and O1 s before (d) and after reaction (e, f).

BET adsorption/desorption curves, which was recorded in the nitrogen atmosphere. The S_{BET} of obtained biochar in this study was maintained at a relatively low level compared to the biochar derived from other feedstocks and pyrolytic conditions according to previous studies [23]. Biochars derived from various crop straw, which were pyrolyzed with 600°C for 3 h. The lower pyrolysis temperature and shorter retention time (400°C, 2 h) brought about the lower surface area of the biochar in this study (Table S1). However, the wood-derived biochar (poplar shaving biochar) pyrolyzed with 600°C for 3 h was not distinguish from the biochar in this study. The higher content of phenolic and aromatic carbons in lignin compared to cellulose [31], formed more fraction of condensed domains. Stiff bonds among cross-links were produced by the aromatic biopolymers. These stiff bonds led the molecular flexibility reduction and decomposition temperature elevation during pyrolysis [32]. Thus, the porosity of straw derived biochar with abundant cellulose was more sensitive to which of the wood-derived biochar with abundant lignin.

3.2. Adsorption kinetics

To study the Cd(II) and Pb(II) adsorption kinetics, the adsorption of such adsorbates on biochar were determined with the contact time (Fig. 5). Results of adsorption kinetics displayed acute rise of both Cd(II) and Pb(II) sequestration in the initial 30 min of the contact time. These sorptions with high efficiency in the initial time were mainly derived by the abundant functional groups on the biochar surface [33]. Subsequently, the increasing trends of the uptake quantity for these adsorbed metal ions slowed down until the plateau after 80 min since the Cd(II) and Pb(II) ions had occupied the superficial functional groups and only the functional groups inside pores were free for binding [34]. After 80 min of the adsorption process, the adsorbate ions obtained equilibrium and kept on a high level as contact time went on. For these observations, biochar could reach an equilibrium state with the retention of Cd(II) and Pb(II) after 80 min. Simultaneously, at every time node of the contact time in this adsorption process, the adsorption quantities of the metal ions always increased with the increasing dosage of biochar. Compared to the biochar material derived from various feedstocks in the previous researches, the straw derived biochar exhibited better adsorption capacity for the Cd(II) and Pb(II) removal in an aqueous solution (Table 1).

To further clarify the mechanism of Cd(II) and Pb(II) removal, two popular kinetics models for practical pollutant adsorption process on biochar were employed [35]. These two popular kinetic models: pseudo-first-order kinetic model and pseudo-second-order kinetic model were generally expressed as below respectively:

$$\ln\left(q_e - q_t\right) = \ln q_e - k_1 t \tag{1}$$

$$\frac{t}{q_t} = \frac{1}{k_2 q_e^2} + \frac{t}{q_e} \tag{2}$$

Both pseudo-first-order kinetic model and pseudo-second-order kinetic could be applied to Cd(II) adsorption as well as Pb(II) adsorption (Table S2). Not a few previous Cd(II) or Pb(II) removal cases by biochar reported that these processes agreed on pseudo-second-order well (Liu et al. [25]). However, much more studies demonstrated that the metal adsorption kinetics fit the pseudo-second-order kinetic best, which was assumed to be caused by valence force

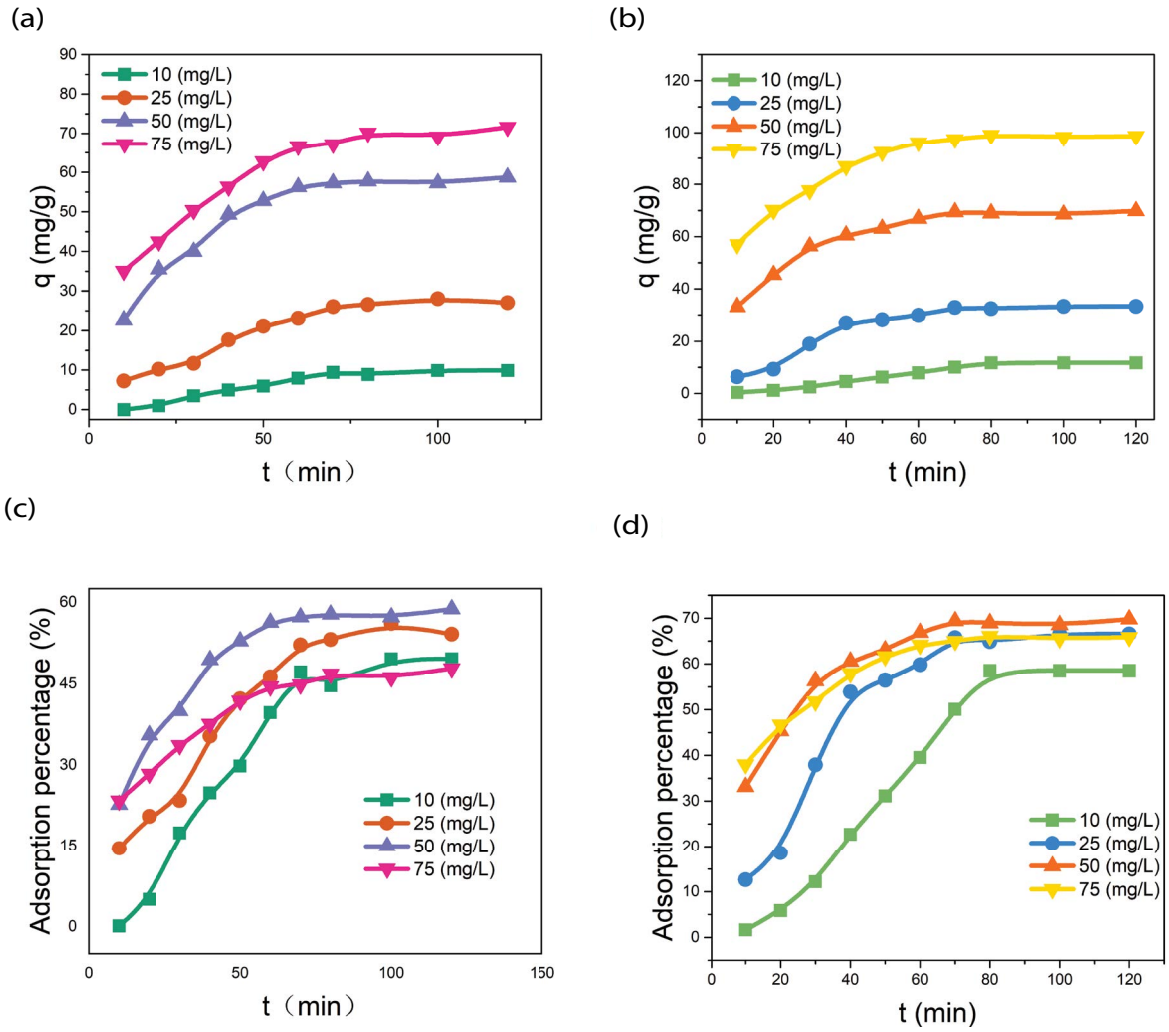

Fig. 5. Adsorption capacity and percentage of Cd(II) (a, c) and Pb(II) (b, d) on biochar as a function of contact time.

Table 1
Adsorption characteristics of Pb(II) and Cd(II) adsorption on various biochar

Feedstock	Pyrolytic temperature (°C)	Retention time	Heavy metal	Adsorption pH	q_{max} (mg g^{-1})	References
Wheat straw	400	2 h	Cd	5.0	16.05	This study
Wheat straw	400	2 h	Pb	5.0	11.70	This study
Scots pine	450	2 h	Cd	7.5–8.5	4.62	[22]
Scots pine	450	2 h	Pb	7.5–8.5	7.51	[22]
Silver birch	450	2 h	Cd	7.5–8.5	4.96	[22]
Silver birch	450	2 h	Pb	7.5–8.5	7.85	[22]
*Miscanthus sacchariflo*rus	300	1 h	Cd	7	11.40	[50]
Miscanthus sacchariflorus	400	1 h	Cd	7	11.99	[50]
Miscanthus sacchariflorus	500	1 h	Cd	7	13.24	[50]
Miscanthus sacchariflorus	600	1 h	Cd	7	12.96	[50]
Pine wood	300	20 min	Pb	4.3	3.89	[53]
Rice husk	300	20 min	Pb	4.3	1.84	[53]

from the electrons exchange in the chemical sorption and chemisorption [6,36–38].

3.3. Effect of pH and ionic strength

As the vital factors to optimize the adsorption process, pH and ionic strength were employed to assess their effect on the Cd(II) or Pb(II) removal. Fig. 3 shows that the adsorbed quantity of the two heavy metal ions varied with both pH and ionic strength in an aqueous solution. Fig. 6a shows that adsorption of Cd(II) rapidly increased with pH in the range of 2.0–7.5 yet the curve was flattened in the pH range of 7.5–10.0. However, the adsorption of Pb(II) could be shaped into a para-curve with a peak at pH of 8.5 (Fig. 6b). The adsorption quantity showed acute elevation and decline in the pH range of 2.0–8.5 and 8.5–10.0 respectively. The functional group such as carboxylate and hydroxyl on biochar surface was held accountable for the increasing metal ion adsorption trend with increasing pH [39,40]. The biochar surface was positively charged since these functional groups were presented and protonated into positive charges at the low pH value. The metal cations were also electrostatically repulsed by the positive charge on the biochar surface. Furthermore, the aqueous cation in the solution such as H^+ and H_3O^+ might compete with the heavy metal adsorbates for the available adsorption sites on the biochar surface [39,40]. With the increasing pH value of the solution, more binding sites were released and the competition between cation contaminants and the protons were alleviated owing to the deprotonation of functional groups [36]. When the solution became strongly alkaline, the surface of biochar showed more negative charges and easy to capture the cations [18]. More OH^- ions in the solution inhibited the shifts of metal ions to biochar through the intensification of competition [25]. Comparably, the capture capacity change peaking at a specific pH value as the Pb adsorption in the study was also supported by the previous cases [36,41,42]. This partial decreasing trends of adsorption capacity with increasing pH might be attributed to the formation of hydroxide complexes [41] Therefore, the optimal pH value for Cd(II) and Pb(II) adsorption are 11 and 8.5 respectively.

On the contrary, the results did not depict a strong correlation between the adsorption capacity and ionic strength of the solution (Fig. 6). This was consistent with some previous Cd(II) and Pb(II) removal cases [9], although some other studies found the aqueous metal ions would affect the equilibrium adsorption capacity for the organic pollutants by biochar [18,43]. Unfortunately, most of these inconsistent results were obtained from simulation wastewater experiment. The effort to eliminate its gap with the actual situation might benefit to better understand the mechanism.

3.4. Adsorption isotherms studie

The adsorption isotherms of Cd(II) and Pb(II) at various temperatures are presented in Fig. 7. The adsorbed quantities of the two metal adsorbates both increased with the rising temperature. These results clearly illustrated that high temperature favored behavior of the metal ion adsorption process. To further explore the quantization and mechanism of the Cd(II) and Pb(II) removal, two empirical quotations: Langmuir and Freundlich model, which fit the experimental data best for heavy metal adsorption by biochar were employed for stimulation [18]. Langmuir's model could be express as: $\frac{1}{q_e}=\frac{1}{q_{\max}}+\frac{1}{bq_{\max}}\frac{1}{C_e}$ in a linear form. $q_{\max}$ (mg g^{-1}) is the maximum amount of adsorbed pollutants by the unit weight of biochar; q_e (mg g^{-1}) indicates the adsorptive heavy metal quantity of unit weight of biochar at equilibrium concentration; b (L mg^{-1}) is the Langmuir constants related to adsorptive energy; C_e represents the equilibrium concentration [10]. Freundlich model could be described as $q_e = K_F C_e^n$ as well as the modified linear form: $\log q_e = \log K_F + n\log C_e K_F$ ($(mg^{1-n}\ L^n)\ g^{-1}$) is the Freundlich constant to evaluate the adsorption capacity; n represents the dependent degree of adsorption process at the equilibrium concentration [44–48]. Table 2 depicts that both Langmuir and Freundlich model fit Cd(II) and Pb(II) adsorption data on biochar according to the plots and R^2 value. Langmuir model is most applicable to the adsorption on monolayer surface while the Freundlich model

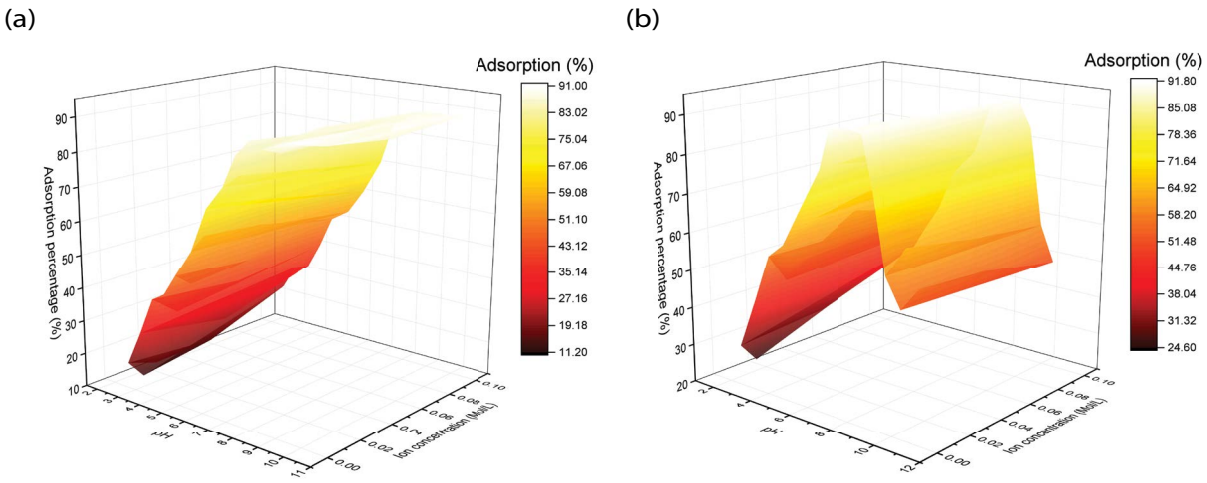

Fig. 6. Effect of pH and foreign ions on Cd(II) (a) and Pb(II) (b) adsorption to biochar.

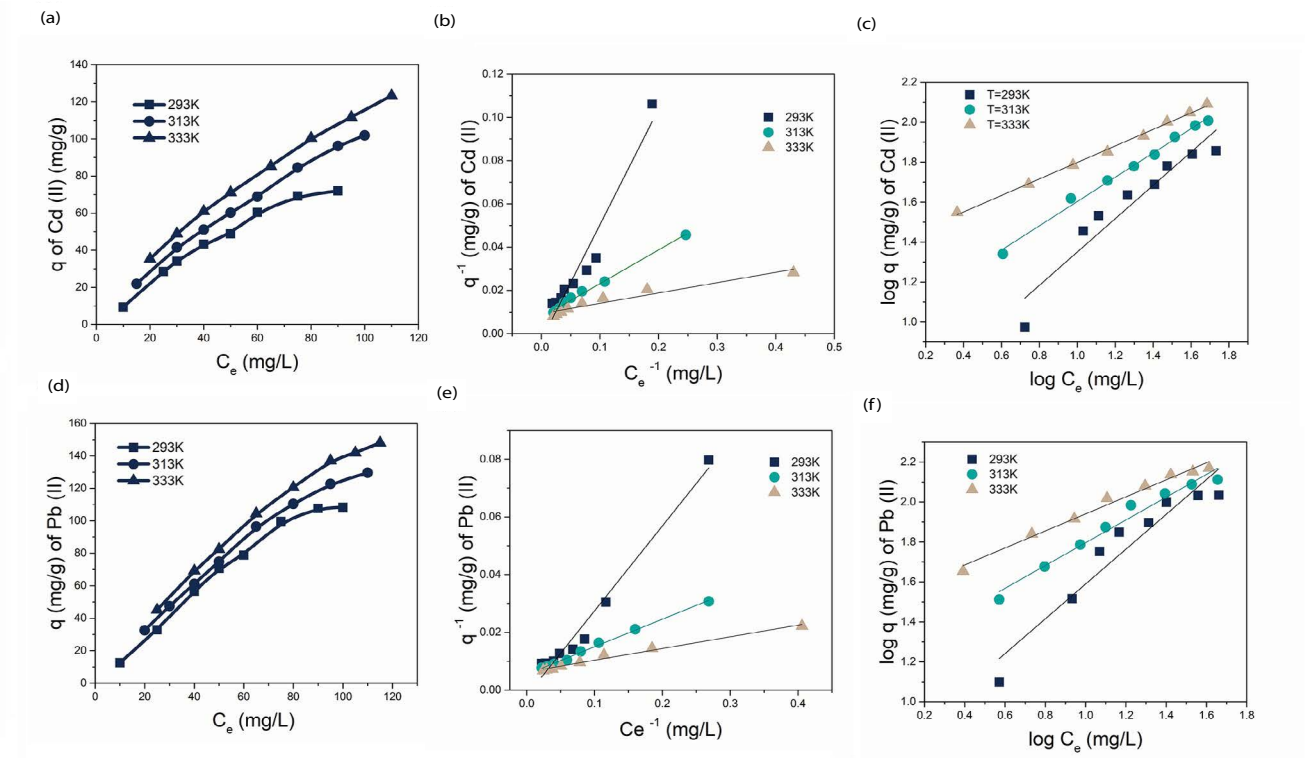

Fig. 7. Isotherm and fitting results of Langmuir and Freundlich adsorption isotherms of Cd(II) (a, c, e) and Pb(II) (b, d, f) adsorption on biochar.

Table 2
Constants of Freundlich and Langmuir isotherm of Pb(II) and Cd(II) adsorption on biochar

Absorbate	T (K)	Freundlich			Langmuir		
		K_F (mg^{1-n} L^n g^{-1})	n	R^2	q_{max} (mg g^{-1})	b (L mg^{-1})	R^2
Cd(II)	293	2.39	0.59	0.9684	125.00	0.028	0.9886
	313	2.71	0.61	0.9928	131.58	0.049	0.9941
	333	4.01	0.41	0.9974	107.53	0.20	0.9290
Pb(II)	293	2.05	0.87	0.9158	400.00	0.12	0.9052
	313	3.41	0.57	0.9705	185.19	0.057	0.9964
	333	4.55	0.43	0.9839	158.73	0.16	0.9845

fits the adsorption on the multi-layer surface and is not restricted to the formation of a monolayer [10,49,50]. In fact, biochar, with the uncertain properties caused by various pyrolysis conditions, could provide both homogeneous and heterogenous partial surfaces [18]. Either the surface superficial functional groups or inside porous structure provided the driving force for the sorption on biochar. Thus, both Langmuir and Freundlich models gave a great fit to either Cd(II) and Pb(II) adsorption by biochar.

3.5. Adsorption thermodynamic calculation

To obtain a better understanding of adsorption thermodynamic, the vital thermodynamic parameters: standard enthalpy ($\Delta H°$), standard entropy ($\Delta S°$), standard Gibbs free energy ($\Delta G°$) were taken into consideration to evaluate the spontaneity of the process (Table 3). These parameters were calculated based on the following equations:

$$K_d = \frac{C_0 - C_e}{C_e}\frac{V}{m} \tag{3}$$

$$\ln K_d = \frac{\Delta S°}{R} - \frac{\Delta H°}{RT} \tag{4}$$

$$\Delta G° = \Delta H° - T\Delta S° \tag{5}$$

where C_0 (mg L^{-1}) represents the initial concentration and C_e (mg L^{-1}) represents the equilibration concentration of the Cd(II) and Pb(II) in aqueous solution respectively; V (mL)

Table 3
Values of thermodynamic parameters for the adsorption of Pb(II) and Cd(II) on biochar

Absorbate	$\Delta H°$ (kJ Mol^{-1})	$\Delta S°$ (J Mol^{-1} K^{-1})	$\Delta G°$ (kJ mol^{-1})		
			293 K	313 K	333 K
Cd(II)	21.31	136.77	–40.05	–42.79	–45.52
Pb(II)	17.20	127.92	–37.46	–40.02	–42.58

and m (g) indicate the volume and mass of biochar as the adsorbent; T (K) and R (8.314 J mol^{-1} K^{-1}) are employed as temperature in Kelvin and the ideal gas constant.

The values of standard enthalpy ($\Delta H°$) exhibited in Table 3 are both positive, which demonstrated that the Cd(II) and Pb(II) adsorptions by biochar were endothermic reactions. The positive values of standard entropy ($\Delta S°$) and negative values of standard Gibbs free energy ($\Delta G°$) also depict these adsorptions as spontaneous processes. This nature indicated the potential of the low cost and operational ease adsorbent to continuously carry out the contaminant removal. These thermodynamic parameters also provided the information of the type of Cd(II) and Pb(II) adsorptions: both physical and chemical adsorptions. Generally, physical adsorption takes van der Waals force while chemical adsorption takes chemical bond as the adsorptive attraction. The $\Delta G°$ of physical adsorption was usually in the interval of –20 to 0 and kJ mol^{-1} and the $\Delta G°$ of chemical adsorption was in the interval of −400 to −80 kJ mol^{-1} [37]. In this study, the Gibbs free energy of Cd(II) and Pb(II) were in the range of –50 to –35 kJ mol^{-1}. This finding implied the Cd(II) and Pb(II) adsorption on biochar combined both physical and chemical adsorptions. The $\Delta H°$ at the low level in both two metal adsorption further proved this assertion. In addition, standard Gibbs free energy ($\Delta G°$) of both Cd(II) and Pb(II) adsorptions showed more negative with the higher temperature, which indicated the spontaneity of the processed were favorable to the temperature. These results were all consistent with the isotherm of these adsorption processes. The endothermic nature, an increase of randomness at the interface and spontaneity favor of the reaction during the adsorption process were extensively identical to the previous metal removal studies using biochar as the adsorbent [23,37,51].

3.6. Practical applicability

To determine the practical applicability of the biochar as the effective adsorbent for aqueous Cd(II) and Pb(II), we also perform the adsorption processes for the wastewater treatment at large scale [52]. The biochar was employed to treat the wastewater with the original Cd(II) concentration of 10.12 mg L^{-1} and Pb(II) concentration of 12.07 mg L^{-1}. The metal removals were practiced under the considered optimal conditions (pH = 8.5 temperature = 25°C). The results depicted 49.87% and 66.35% Pb(II) as the Cd(II) and Pb(II) removal percentages respectively (Table S3). The simulant wastewater with the same original Cd(II) and Pb(II) concentration was also treated by biochar. The adsorption percentages were 38.59% for Cd(II) and 59.64% for Pb(II) respectively. Biochar showed even higher contaminant removal efficiency in the actual wastewater than the simulant wastewater. This finding indicated practical applicability of the biochar as the effective adsorbent for Cd(II) and Pb(II) removal in the actual wastewater.

4. Conclusion

This study provides a better understanding of the Cd(II) and Pb(II) adsorption on biochar through a systematic survey. Our findings demonstrated that the complex surface, porous and permeable structure of biochar played a great role in metal adsorption. Both the two metal removal processes agreed well to the pseudo-first-order and pseudo-second-order either. The adsorption efficiency reached an equilibrium state after 80 min. The adsorption capacity for Cd(II) on biochar was found to be positively dependent on the pH value in the range of 2.0–7.5 and maintaining a number of high level in the range of 7.5–10.0 while adsorption capacity for Pb(II) was positively and negatively correlated to the pH value in the range of 2.0–8.5 and 8.5–10.0 respectively. However, in the extensive pH range, both the Cd(II) and Pb(II) adsorption were independent of the ionic strength. The isotherm results indicated that Langmuir and Freundlich's model supplied a fit for the adsorption of the metal ions because of the superficial functional groups and porous structure of biochar. The thermodynamic parameters reflected natures of the Cd(II) and Pb(II) adsorption reactions such as endothermy, spontaneity favor and increase of randomness at the interface. The adsorption type of these adsorptions were also revealed as the combination of physical and chemical adsorption. This work reveals that biochar is a promising proper adsorbent for the efficient elimination of metal ions from aqueous solutions.

References

[1] D. Hou, J. He, C.W. Lü, L.M. Ren, Q.Y. Fan, J.H. Wang, Z.L. Xie, Distribution characteristics and potential ecological risk assessment of heavy metals (Cu, Pb, Zn, Cd) in water and sediments from Lake Dalinouer, China, Ecotoxicol. Environ. Saf., 93 (2013) 135–144.
[2] S.P. Cheng, Heavy metal pollution in China: origin, pattern and control, Environ. Sci. Pollut. Res., 10 (2003) 192–198.
[3] D.K. Singh, S. Mishra, Synthesis, characterization and removal of Cd(II) using Cd(II)-ion imprinted polymer, J. Hazard. Mater., 164 (2009) 1547–1551.
[4] Y.C. Lu, J. He, G.S. Luo, An improved synthesis of chitosan bead for Pb(II) adsorption, Chem. Eng. J., 226 (2013) 271–278.
[5] G.X. Zhao, X.M. Ren, X. Gao, X.L. Tan, J.X. Li, C.L. Chen, Y.Y. Huang, X.K. Wang, Removal of Pb(II) ions from aqueous solutions on few-layered graphene oxide nanosheets, Dalton Trans., 40 (2011) 10945–10952.
[6] G.D. Sheng, S.W. Wang, J. Hu, Y. Lu, J.X. Li, Y.H. Dong, X.K. Wang, Adsorption of Pb(II) on diatomite as affected via aqueous solution chemistry and temperature, Colloids Surf., A, 339 (2009) 159–166.

[7] A. Azimi, A. Azari, M. Rezakazemi, M. Ansarpour, Removal of heavy metals from industrial wastewaters: a review, ChemBioEng Rev., 4 (2017) 37–59.
[8] Q.W. Zhou, B.H. Liao, L. Lin, W.W. Qiu, Z.G. Song, Adsorption of Cu(II) and Cd(II) from aqueous solutions by ferromanganese binary oxide–biochar composites, Sci. Total Environ., 615 (2018) 115–122.
[9] Q. Liao, S.R. Yan, W.S. Linghu, Y.L. Zhu, R.P. Shen, F. Ye, G.F. Feng, L.J. Dong, A.M. Asiri, H.M. Marwani, D. Xu, X.L. Wu, X. Li, Impact of key geochemical parameters on the highly efficient sequestration of Pb(II) and Cd(II) in water using g-C_3N_4 nanosheets, J. Mol. Liq., 258 (2018) 40–47.
[10] M.I. Inyang, B. Gao, Y. Yao, Y.W. Xue, A. Zimmerman, A. Mosa, P. Pullammanappallil, Y.S. Ok, X.D. Cao, A review of biochar as a low-cost adsorbent for aqueous heavy metal removal, Crit. Rev. Env. Sci. Technol., 46 (2015) 406–433.
[11] X.D. Cao, L. Ma, Y. Liang, B. Gao, W. Harris, Simultaneous immobilization of lead and atrazine in contaminated soils using dairy-manure biochar, Environ. Sci. Technol., 45 (2011) 4884–4889.
[12] X.L. Dong, L.Q. Ma, Y.C. Li, Characteristics and mechanisms of hexavalent chromium removal by biochar from sugar beet tailing, J. Hazard. Mater., 190 (2011) 909–915.
[13] S.S. Wang, B. Gao, A.R. Zimmerman, Y.C. Li, L. Ma, W.G. Harris, K.W. Migliaccio, Removal of arsenic by magnetic biochar prepared from pinewood and natural hematite, Bioresour. Technol., 175 (2015) 391–395.
[14] M. Ahmad, A.U. Rajapaksha, J.E. Lim, M. Zhang, N. Bolan, D. Mohan, M. Vithanage, S.S. Lee, Y.S. Ok, Biochar as a sorbent for contaminant management in soil and water: a review, Chemosphere, 99 (2014) 19–33.
[15] M. Ahmad, S.S. Lee, X.M. Dou, D. Mohan, J.-K. Sung, J.E. Yang, Y.S. Ok, Effects of pyrolysis temperature on soybean stover- and peanut shell-derived biochar properties and TCE adsorption in water, Bioresour. Technol., 118 (2012) 536–544.
[16] X.D. Cao, W. Harris, Properties of dairy-manure-derived biochar pertinent to its potential use in remediation, Bioresour. Technol., 101 (2010) 5222–5228.
[17] K. Sun, K. Ro, M.X. Guo, J. Novak, H. Mashayekhi, B.S. Xing, Sorption of bisphenol A, 17α-ethinyl estradiol and phenanthrene on thermally and hydrothermally produced biochars, Bioresour. Technol., 102 (2011) 5757–5763.
[18] X.F. Tan, Y.G. Liu, G.M. Zeng, X. Wang, X.J. Hu, Y.L. Gu, Z.Z. Yang, Application of biochar for the removal of pollutants from aqueous solutions, Chemosphere, 125 (2015) 70–85.
[19] J.-H. Kwak, S. Islam, S.Y. Wang, S.A. Messele, M.A. Naeth, M.G. El-Din, S.X. Chang, Biochar properties and lead(II) adsorption capacity depend on feedstock type, pyrolysis temperature, and steam activation, Chemosphere, 231 (2019) 393–404.
[20] Y.X. Li, G.P. Pei, X.L. Qiao, Y. Zhu, H. Li, Remediation of cadmium contaminated water and soil using vinegar residue biochar, Environ. Sci. Pollut. Res. Int., 25 (2018) 15754–15764.
[21] M.A. Naeem, M. Imran, M. Amjad, G. Abbas, M. Tahir, B. Murtaza, A. Zakir, M. Shahid, L. Bulgariu, I. Ahmad, Batch and column scale removal of cadmium from water using raw and acid activated wheat straw biochar, Water, 11 (2019) 1438, https://doi.org/10.3390/w11071438.
[22] J. Komkiene, E. Baltrenaite, Biochar as adsorbent for removal of heavy metal ions [cadmium(II), copper(II), lead(II), zinc(II)] from aqueous phase, Int. J. Environ. Sci. Technol., 13 (2016) 471–482.
[23] J.K. Sun, F. Lian, Z.Q. Liu, L.Y. Zhu, Z.G. Song, Biochars derived from various crop straws: characterization and Cd(II) removal potential, Ecotoxicol. Environ. Saf., 106 (2014) 226–231.
[24] Q. Liao, D.S. Zou, W. Pan, W.S. Linghu, R.P. Shen, X. Li, A.M. Asiri, K.A. Alamry, G.D. Sheng, L. Zhan, X.L. Wu, Highly efficient capture of Eu(III), La(III), Nd(III), Th(IV) from aqueous solutions using g-C_3N_4 nanosheets, J. Mol. Liq., 252 (2018) 351–361.
[25] N. Liu, Y.T. Zhang, C. Xu, P. Liu, J. Lv, Y.Y. Liu, Q.Y. Wang, Removal mechanisms of aqueous Cr(VI) using apple wood biochar: a spectroscopic study, J. Hazard. Mater., 384 (2020) 121371, https://doi.org/10.1016/j.jhazmat.2019.121371.
[26] A. Méndez, A.M. Tarquis, A. Saa-Requejo, F. Guerrero, G. Gascó, Influence of pyrolysis temperature on composted sewage sludge biochar priming effect in a loamy soil, Chemosphere, 93 (2013) 668–676.
[27] T. Chi, J. Zuo, F.L. Liu, Performance and mechanism for cadmium and lead adsorption from water and soil by corn straw biochar, Front. Environ. Sci. Eng., 11 (2017), https://doi.org/10.1007/s11783-017-0921-y.
[28] C.H. Chia, B. Gong, S.D. Joseph, C.E. Marjo, P. Munroe, A.M. Rich, Imaging of mineral-enriched biochar by FTIR, Raman and SEM–EDX, Vib. Spectrosc., 62 (2012) 248–257.
[29] H.H. Lyu, J.C. Tang, Y. Huang, L.S. Gai, E.Y. Zeng, K. Liber, Y.Y. Gong, Removal of hexavalent chromium from aqueous solutions by a novel biochar supported nanoscale iron sulfide composite, Chem. Eng. J., 322 (2017) 516–524.
[30] M. Genovese, J.H. Jiang, K. Lian, N. Holm, High capacitive performance of exfoliated biochar nanosheets from biomass waste corn cob, J. Mater. Chem. A, 3 (2015) 2903–2913.
[31] X.L. Wang, B.S. Xing, Importance of structural makeup of biopolymers for organic contaminant sorption, Environ. Sci. Technol., 41 (2007) 3559–3565.
[32] K.D. Young, E.J. Leboeuf, Glass transition behavior in a peat humic acid and an aquatic fulvic acid, Environ. Sci. Technol., 34 (2000) 4549–4553.
[33] A.R. Lucaci, D. Bulgariu, I. Ahmad, G. Lisă, A.M. Mocanu, L. Bulgariu, Potential use of biochar from various waste biomass as biosorbent in Co(II) removal processes, Water, 11 (2019) 1565, https://doi.org/10.3390/w11081565.
[34] L.B. Escudero, P.Y. Quintas, R.G. Wuilloud, G.L. Dotto, Recent advances on elemental biosorption, Environ. Chem. Lett., 17 (2018) 409–427.
[35] X.L. Tan, X.M. Ren, C.L. Chen, X.K. Wang, Analytical approaches to the speciation of lanthanides at solid-water interfaces, TrAC, Trends Anal. Chem., 61 (2014) 107–132.
[36] H.L. Lu, W.H. Zhang, Y.X. Yang, X.F. Huang, S.Z. Wang, R.L. Qiu, Relative distribution of Pb^{2+} sorption mechanisms by sludge-derived biochar, Water Res., 46 (2012) 854–862.
[37] Z. Liu, F.S. Zhang, Removal of lead from water using biochars prepared from hydrothermal liquefaction of biomass, J. Hazard. Mater., 167 (2009) 933–939.
[38] D. Kołodyńska, R. Wnętrzak, J.J. Leahy, M.H.B. Hayes, W. Kwapiński, Z. Hubicki, Kinetic and adsorptive characterization of biochar in metal ions removal, Chem. Eng. J., 197 (2012) 295–305.
[39] T.-K. Oh, B. Choi, Y. Shinogi, J. Chikushi, Effect of pH conditions on actual and apparent fluoride adsorption by biochar in aqueous phase, Water Air Soil Pollut., 223 (2012) 3729–3738.
[40] T.M. Abdel-Fattah, M.E. Mahmoud, S.B. Ahmed, M.D. Huff, J.W. Lee, S. Kumar, Biochar from woody biomass for removing metal contaminants and carbon sequestration, J. Ind. Eng. Chem., 22 (2015) 103–109.
[41] X. Chen, G. Chen, L. Chen, Y. Chen, J. Lehmann, M.B. McBride, A.G. Hay, Adsorption of copper and zinc by biochars produced from pyrolysis of hardwood and corn straw in aqueous solution, Bioresour. Technol., 102 (2011) 8877–8884.
[42] X.-j. Tong, J.-y. Li, J.-h. Yuan, R.-k. Xu, Adsorption of Cu(II) by biochars generated from three crop straws, Chem. Eng. J., 172 (2011) 828–834.
[43] M. Jia, F. Wang, Y. Bian, X. Jin, Y. Song, F.O. Kengara, R. Xu, X. Jiang, Effects of pH and metal ions on oxytetracycline sorption to maize-straw-derived biochar, Bioresour. Technol., 136 (2013) 87–93.
[44] B. Hu, G. Chen, C. Jin, J. Hu, C. Huang, J. Sheng, G. Sheng, J. Ma, Y. Huang, Macroscopic and spectroscopic studies of the enhanced scavenging of Cr(VI) and Se(VI) from water by titanate nanotube anchored nanoscale zero-valent iron, J. Hazard. Mater., 336 (2017) 214–221.
[45] B.W. Hu, F. Ye, C.G. Jin, X.X. Ma, C.C. Huang, G.D. Sheng, J.Y. Ma, X.K. Wang, Y.Y. Huang, The enhancement roles of layered double hydroxide on the reductive immobilization

of selenate by nanoscale zero valent iron: macroscopic and microscopic approaches, Chemosphere, 184 (2017) 408–416.
[46] B. Hu, C. Huang, X. Li, G. Sheng, H. Li, X. Ren, J. Ma, J. Wang, Y. Huang, Macroscopic and spectroscopic insights into the mutual interaction of graphene oxide, Cu(II), and Mg/Al layered double hydroxides, Chem. Eng. J., 313 (2017) 527–534.
[47] K. Chang, Y. Sun, F. Ye, X. Li, G. Sheng, D. Zhao, W. Linghu, H. Li, J. Liu, Macroscopic and molecular study of the sorption and co-sorption of graphene oxide and Eu(III) onto layered double hydroxides, Chem. Eng. J., 325 (2017) 665–671.
[48] B. Hu, F. Ye, X. Ren, D. Zhao, G. Sheng, H. Li, J. Ma, X. Wang, Y. Huang, X-ray absorption fine structure study of enhanced sequestration of U(VI) and Se(IV) by montmorillonite decorated with zero-valent iron nanoparticles, Environ. Sci.: Nano, 3 (2016) 1460–1472.
[49] X.J. Hu, J.S. Wang, Y.G. Liu, X. Li, G.M. Zeng, Z.L. Bao, X.X. Zeng, A.W. Chen, F. Long, Adsorption of chromium (VI) by ethylenediamine-modified cross-linked magnetic chitosan resin: isotherms, kinetics and thermodynamics, J. Hazard. Mater., 185 (2011) 306–314.
[50] W.-K. Kim, T.Y. Shim, Y.-S. Kim, S.H. Hyun, C.K. Ryu, Y.-K. Park, J.H. Jung, Characterization of cadmium removal from aqueous solution by biochar produced from a giant *Miscanthus* at different pyrolytic temperatures, Bioresour. Technol., 138 (2013) 266–270.
[51] G.K. Parshetti, S. Chowdhury, R. Balasubramanian, Hydrothermal conversion of urban food waste to chars for removal of textile dyes from contaminated waters, Bioresour. Technol., 161 (2014) 310–319.
[52] I.S. Badescu, D. Bulgariu, I. Ahmad, L. Bulgariu, Valorisation possibilities of exhausted biosorbents loaded with metal ions – a review, J. Environ. Manage., 224 (2018) 288–297.
[53] L. Qian, B. Chen, Dual role of biochars as adsorbents for aluminum: the effects of oxygen-containing organic components and the scattering of silicate particles, Environ. Sci. Technol., 47 (2013) 8759–8768.

Supporting information

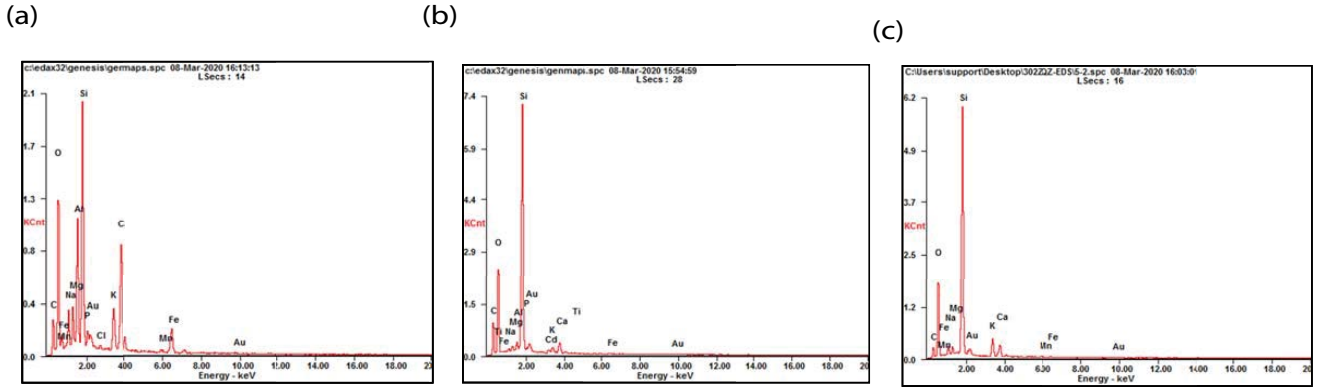

Fig. S1. SEM corresponding energy-dispersive X-ray spectroscopy (EDS) spectra (right) of biochar before (a) and after Cd(II) and Pb(II) reaction (b and c).

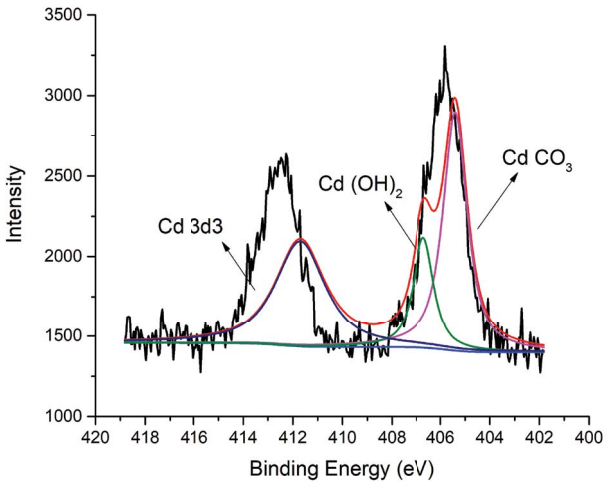

Fig. S2. High-resolution X-ray photoelectron spectroscopy (XPS) spectra of Cd after the reaction.

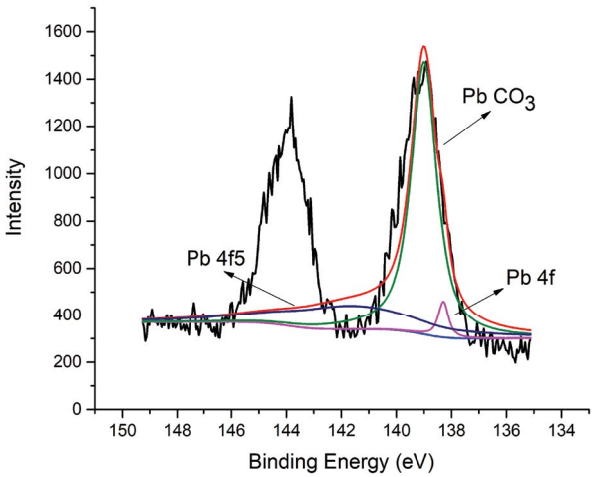

Fig. S3. High-resolution X-ray photoelectron spectroscopy (XPS) spectra of Pb after the reaction.

Table S1
BET surface area of the obtained biochar in this and previous studies

Biochar feedstock	BET surface area ($m^2\ g^{-1}$)
Rice straw (This study)	25.666
Rice straw	156.2
Cotton straw	49.4
Wheat straw	183.3
Corn straw	70.0
Poplar shaving	37.7

Table S2
Constants of pseudo-first-order and pseudo-second-order stimulation of Pb(II) and Cd(II) adsorption on biochar

Absorbate	C_0 (mg L^{-1})	Pseudo-first-order			Pseudo-second-order		
		q_e (mg g^{-1})	K_1	R^2	q_e (mg g^{-1})	K_2	R^2
Cd(II)	10	16.0572	0.00955	0.9066	27.7160	0.0002008	0.9016
	25	31.5387	0.02095	0.9586	44.3248	0.0003777	0.9467
	50	59.1579	0.04412	0.9840	71.3855	0.0007027	0.9681
	75	69.8344	0.04873	0.9236	82.1379	0.0007412	0.9644
Pb(II)	10	30.8597	0.00466	0.9032	59.3795	0.0000405	0.9018
	25	37.2627	0.02506	0.9292	51.5065	0.0003963	0.9035
	50	69.0858	0.05661	0.9813	80.2583	0.0009421	0.9795
	75	97.0312	0.06806	0.9040	109.6643	0.0008897	0.9688

Table S3
Practical applicability in actual wastewater

Metal	Original metal concentration in actual wastewater (mg L^{-1})	Removal percentages in actual wastewater (%)	Removal percentages in simulant wastewater
Cd(II)	10.12	49.87	38.59
Pb(II)	12.07	66.35	59.64